The Deep-Ocean Heat Uptake in Transient Climate Change

BOYIN HUANG, PETER H. STONE, AND ANDREI P. SOKOLOV

Joint Program on the Science and Policy of Global Change, Massachusetts Institute of Technology, Cambridge, Massachusetts

IGOR V. KAMENKOVICH

Department of Atmospheric Sciences, University of Washington, Seattle, Washington

(Manuscript received 20 June 2002, in final form 3 November 2002)

ABSTRACT

The deep-ocean heat uptake (DOHU) in transient climate changes is studied using an ocean general circulation model (OGCM) and its adjoint. The model configuration consists of idealized Pacific and Atlantic basins. The model is forced with the anomalies of surface heat and freshwater fluxes from a global warming scenario with a coupled model using the same ocean configuration. In the global warming scenario, CO_2 concentration increases 1% yr^{-1}. The heat uptake calculated from the coupled model and from the adjoint are virtually identical, showing that the heat uptake by the OGCM is a linear process.

After 70 yr the ocean heat uptake is almost evenly distributed within the layers above 200 m, between 200 and 700 m, and below 700 m (about 20×10^{22} J in each). The effect of anomalous surface freshwater flux on the DOHU is negligible. Analysis of the Coupled Model Intercomparison Project (CMIP-2) data for the same global warming scenario shows that qualitatively similar results apply to coupled atmosphere–ocean GCMs.

The penetration of surface heat flux to the deep ocean in the OGCM occurs mainly in the North Atlantic and the Southern Ocean, since both the sensitivity of DOHU to the surface heat flux and the magnitude of anomalous surface heat flux are large in these two regions. The DOHU relies on the reduction of convection and Gent–McWilliams–Redi mixing in the North Atlantic, and the reduction of Gent–McWilliams–Redi mixing in the Southern Ocean.

1. Introduction

The study of Levitus et al. (2000) shows that the World Ocean has warmed since the mid-1950s. The change of deep-ocean temperature may be affected by the long-term climate variability. However, studies based on coupled atmosphere–ocean general circulation models (AOGCMs) indicate that the detected warming is consistent with that expected due to an increase of greenhouse gases (Levitus et al. 2001; Barnett et al. 2001).

Studies from the Coupled Model Intercomparison Project (CMIP-2) show that the warming due to increasing greenhouse gases leads to an increase of downward net surface heat flux into the ocean. In addition, the warming is accompanied by an increase of freshwater flux into the ocean in higher latitudes, but out of the ocean in midlatitudes (Figs. 1c,d). As a result, the thermohaline circulation slows down in most of the models. However, the relative role of the changes in surface heat and freshwater fluxes is unclear. Dixon et al. (1999) show that in the Geophysical Fluid Dynamics Laboratory (GFDL) model the weakening of the thermohaline circulation is mainly caused by the increase of freshwater flux into the ocean. Their result seems to indicate the importance of freshwater flux to the thermohaline circulation as in Weaver et al. (1993), Rahmstorf (1995, 1996), Wiebe and Weaver (1999), and Zhang et al. (1999). On the other hand, the studies of Mikolajewicz and Voss (2000), Thorpe et al. (2001), and Kamenkovich et al. (2002) indicate that the increase of net surface heat flux is the dominant factor in the slowdown of the thermohaline circulation.

From the viewpoint of deep-ocean heat uptake (DOHU), the slowdown of the thermohaline circulation may cool the deep ocean due to reduced downward heat transport (Huang et al. 2003, their Fig. 3). What then causes the warming of the global deep ocean? As indicated in Huang et al. (2003), the DOHU in equilibrium may be sensitive to both the surface heat and freshwater fluxes. But, it is not clear whether they play an important role in the DOHU in transient climate changes. We will address this question by combining adjoint sensitivities to the surface heat and freshwater fluxes with anomalies of these fluxes from coupled AOGCM simulations when greenhouse gases increase. In an earlier paper, we re-

Corresponding author address: Boyin Huang, The Center for Research on the Changing Earth System (CRCES), 10211 Wincopin Circle, Suite 240, Columbia, MD 21044.
E-mail: bhuang@wind.mit.edu

ported on the equilibrium sensitivities (Huang et al. 2003), but here we report on and make use of the transient sensitivities. Section 2 is a brief description of the Massachusetts Institute of Technology (MIT) OGCM and its adjoint. The roles of anomalous surface heat and freshwater fluxes in DOHU in the MIT OGCM and the CMIP-2 models are compared in section 3. The sensitivity and mechanisms resulting in the increase of DOHU are studied in section 4. The spatial variations of DOHU due to the increase of greenhouse gases are presented in section 5. The DOHU below 200 and 700 m is briefly compared in section 6. Our conclusions are given in section 7.

2. Model

We use the MIT OGCM (Marshall et al. 1997) and its adjoint (Giering 1999; Marotzke et al. 1999) with an idealized Pacific and Atlantic connected by an idealized Drake Passage (Huang et al. 2003; Kamenkovich et al. 2002). The longitudinal resolution is 1° near the western and eastern boundaries, but 4° in the central ocean. The finer resolution near the boundaries enables the simulation of the western boundary current more realistically. The latitudinal resolution is 4°. The ocean depth is 4.5 km, which is discretized into 15 levels. The thickness between levels is 50 m near the surface, and increases to 550 m at the bottom. The diapycnal (vertical) diffusivity is set to 5×10^{-5} m^2 s^{-1} for temperature and salinity. The isopycnal diffusivity is set to 10^3 m^2 s^{-1}, and the effect of mesoscale eddies on tracers is calculated based on Gent and McWilliams (1990) and Redi (1982). Isopycnal and thickness diffusivities are assumed to be the same, and the mixing due to these diffusions is referred to as Gent–McWilliams–Redi (GMR) mixing.

The ocean is spun up for 5000 yr by applying mixed boundary conditions:

$$\rho c_p \frac{dT_1}{dt}\Delta Z_1 = Q_S = \rho c_p \frac{\mathrm{SST} - T_1}{\tau}\Delta Z_1 + F_H, \quad (1)$$

$$\frac{dS_1}{dt} = \frac{S_0}{\Delta Z_1}F_S, \quad (2)$$

$$F_S = E - P - R, \quad (3)$$

where SST is observed monthly sea surface temperature. Here, T_1, S_1, and ΔZ_1 are the temperature, salinity, and thickness, respectively, of the first model layer; τ is a restoring time of 30 days; F_H is observed monthly net surface heat flux (positive downward) and F_S is observed annual freshwater flux in unit of m s^{-1}, both from Jiang et al. (1999); F_S is defined as the difference between evaporation, precipitation, and river runoff. SST, F_H, and F_S are zonally averaged in the Pacific and Atlantic separately, and S_0 is the standard salinity of 35 psu.

After the spinup, the surface boundary condition of temperature is reset to the flux boundary condition as follows:

$$\rho c_p \frac{dT_1}{dt}\Delta Z_1 = \overline{Q}_S, \quad (4)$$

where $\overline{Q}_S$ is monthly mean surface heat flux diagnosed from the last 10 yr of the spinup run using (1). The flux boundary condition of (4) is very important in studying the adjoint sensitivity of DOHU to the surface heat flux. Otherwise, the perturbation added in (1) may immediately be damped by the restoring term except at the higher latitudes (Huang et al. 2003).

In contrast to the OGCM, which is integrated from an initial state to a final state of one's interest, the adjoint of OGCM is integrated from the final state to the initial state (Marotzke et al. 1999). The purpose of the adjoint is to calculate the sensitivities of a so-called cost function $F_c(n)$ at a timescale of n years to a set of model control parameters P_m:

$$S_m(n, x, y, z) = \frac{\partial F_c(n)}{\partial P_m(x, y, z)}, \qquad m = 1, M, \quad (5)$$

by applying the tangent linear and adjoint compiler (Giering 1999), which measures the change of the so-called cost function after a *constant* anomalous forcing maintained for n years at a specific location. The advantage of the adjoint is that the sensitivity to many parameters ($M \gg 1$) can be calculated by one adjoint simulation. If one wishes to calculate these sensitivities by integrating the OGCM, only one parameter can be perturbed at one grid point each time. Therefore, it is impossible to calculate these sensitivities for all parameters at all grid points. In our study, we choose the global averaged temperature below 700 m as a cost function:

$$F_c = \overline{T}(n, z < -700 \text{ m}), \quad (6)$$

and choose surface heat flux (Q_S) and freshwater flux ($F_S = E - P - R$) as control parameters. The change of F_c (in unit of K) is referred to as DOHU unless otherwise specified. We ran the adjoint model for 70 yr, and calculated the sensitivities of DOHU to Q_S and F_S for the timescales from 1 to 70 yr as indicated in (5). Using these sensitivities, we will demonstrate that the impact of anomalous freshwater flux on the DOHU is negligible, and its effect on the thermohaline circulation is small as in Mikolajewicz and Voss (2000), Thorpe et al. (2001), and Kamenkovich et al. (2003). We will not discuss the role of anomalous wind stress due to its small effect on the DOHU and the thermohaline circulation (Dixon et al. 1999; Mikolajewicz and Voss 2000; Bugnion 2001).

3. Role of surface heat and freshwater fluxes in the MIT model

a. Comparison using the adjoint model

To estimate the role of surface heat and freshwater fluxes in the DOHU below 700 m in a global warming

TABLE 1. Estimated ocean heat uptake (K) in different models at the timescale of 70 yr. Here $\partial\overline{T}/\partial Q_S$ and $\partial\overline{T}/\partial F_S$ are the adjoint sensitivities of DOHU to surface heat and freshwater flux, respectively, and ΔQ_S, $\Delta F_S = \Delta(E - P - R)$, and $\Delta\overline{T}$ are the anomalies between perturbation and control runs. A 1° change of average temperature below 700 m (200 m) represents a DOHU of 3.7 (4.2) $\times 10^{24}$ J.

	Below 700 m			Below 200 m		
	$\frac{\partial\overline{T}}{\partial Q_S}\Delta Q_S$	$\frac{\partial\overline{T}}{\partial F_S}\Delta F_S$	$\Delta\overline{T}$	$\frac{\partial\overline{T}}{\partial Q_S}\Delta Q_S$	$\frac{\partial\overline{T}}{\partial F_S}\Delta F_S$	$\Delta\overline{T}$
KSS model	0.052	−0.0010	0.053	0.094	0.00020	0.098
BMRC	0.053	0.00062	0.042	0.110	0.0024	0.082
ECHAM3	0.033	0.0012	0.029	0.062	0.0022	0.064
GFDL	0.065	0.0019	0.085	0.130	0.0027	0.153
GISS	0.048	0.0011	0.071	0.092	0.00087	0.114
IAP	0.040	−0.000043	0.028	0.092	0.00099	0.088
NCAR-CSM	0.037	N/A	0.043	0.068	N/A	0.082
HadCM2	0.035	0.0021	0.058	0.074	0.0029	0.104

scenario, we use the anomalies of net surface heat flux (Q_n, $n = 1, 70$, positive downward) and freshwater flux ($F_n = \delta E_n - \delta P_n - \delta R_n$) when CO_2 concentration increases at 1% yr^{-1} for 70 yr. Here Q_n and F_n are averaged monthly from Kamenkovich et al. (2002, hereafter KSS). KSS use the modular ocean model of the GFDL coupled with a zonal mean statistical–dynamical atmosphere. The ocean configuration of KSS is the same as in our study.

The DOHU at a timescale of n years forced by the anomaly of surface heat and freshwater fluxes can be estimated as

$$\Delta\overline{T}_n = \Delta T_n^Q + \Delta T_n^F = \sum_{i=1}^{n}\sum_{x,y}\left[\frac{\partial\overline{T}_{n-i+1}}{\partial Q_S(x,y)}\Delta Q_i(x,y) + \frac{\partial\overline{T}_{n-i+1}}{\partial F_S(x,y)}\Delta F_i(x,y)\right], \quad (7)$$

where

$$\Delta Q_n = Q_n - Q_{n-1}, \quad (8)$$

$$\Delta F_n = F_n - F_{n-1}, \qquad n = 1, 70, \quad (9)$$

and Q_n and F_n are the anomalies of surface heat and freshwater ($E - P - R$) fluxes from KSS (Fig. 1). The surface heat flux anomaly at year 70 is about 5 W m^{-2} in the Southern Ocean south of 45°S, and about 20 W m^{-2} in the North Atlantic north of 50°N (Figs. 1a,b). The surface heat flux anomaly is very weak north of 30°S in the Pacific, and between 30°S and 30°N in the Atlantic. The anomaly of precipitation dominates over that of evaporation by about 2 cm yr^{-1} in the Southern Ocean south of 50°S, about 5 cm yr^{-1} in the equatorial ocean between 10°S and 10°N in both the Pacific and the Atlantic, about 5 cm yr^{-1} in the North Pacific north of 40°N, and about 10 cm yr^{-1} in the North Atlantic north of 40°N (Figs. 1c,d). But the anomaly of evaporation dominates over that of precipitation by about 5 cm yr^{-1} between 40° and 10°S and between 10° and 40°N in both the Pacific and the Atlantic.

We find that due to the anomalies of surface heat flux and freshwater flux ($E - P - R$) at the timescale of 70 yr, the DOHU is 0.052 and −0.001 K, respectively (Table 1; KSS model). This indicates that the heat flux anomaly plays a dominant role over the freshwater flux anomaly in the DOHU below 700 m at this timescale in the global warming simulation of KSS. The effect of anomalous freshwater flux is negligible. We note that a 1° change of average temperature below 700 m represents a DOHU of 3.7×10^{24} J. The actual heat uptake calculated from the output of the KSS model simulation of the global warming scenario is 0.053 K (ΔT in Table 1). The closeness to the value calculated using the adjoint sensitivities, 0.052 K, shows that the heat uptake in the KSS model is, to a very good approximation, a linear process.

b. Comparison using OGCM

To further verify the predominance of the surface heat flux anomaly in the DOHU in the global warming scenario, we designed a set of simulations with the MIT OGCM by introducing additional heat (Q_n) and freshwater (F_n) flux anomalies from KSS:

$$\rho c_p\frac{dT_1}{dt}\Delta Z_1 = Q_S = \overline{Q}_S + Q_n, \quad (10)$$

$$\frac{dS_1}{dt} = \frac{S_0}{\Delta Z_1}(F_S + F_n), \qquad n = 1, 70, \quad (11)$$

where $\overline{Q}_S$ and F_S are the climatological surface heat and freshwater fluxes as in (4) and (2). The simulations are run for 70 yr in the following conditions: (i) control run without anomalies of surface heat and freshwater fluxes, $Q_n = F_n = 0$, (ii) with heat flux anomaly only, $F_n = 0$, (iii) with freshwater flux anomaly only, $Q_n = 0$, and (iv) with both heat and freshwater flux anomalies, $Q_n \neq 0$ and $F_n \neq 0$.

The DOHU below 700 m is calculated by the difference between the perturbation and control simulations using

$$\Delta\overline{T}_n = \overline{T}_n^{\text{pert}}(z < -700\text{ m}) - \overline{T}_n^{\text{ctrl}}(z < -700\text{ m}). \quad (12)$$

The results show that the DOHU is about 0.05, −0.001,

and 0.05 K (or 20, −1, and 19 × 10^{22} J), respectively, when forced with the surface heat flux anomaly, the freshwater flux ($E - P - R$) anomaly, and the anomalies of both the surface heat and freshwater fluxes from KSS. The dominant effect of anomalous surface heat flux on DOHU is consistent with the estimate using the adjoint sensitivities.

The anomalous heat flux increases the DOHU by the reduction of convection and GMR mixing (see section 4b for details), and decreases the thermohaline circulation. The anomalous freshwater flux ($E - P - R$) in the high latitudes of the North Atlantic decreases the DOHU, albeit slightly, owing to the slowdown of the thermohaline circulation. The effect of freshwater flux anomaly in the high latitudes is partially cancelled by that in the subtropical Atlantic (Fig. 1d; KSS), as indicated in Latif et al. (2000). The reason is that the sensitivity of DOHU to the freshwater flux is positive over the entire Atlantic (not shown). Therefore, the positive anomaly of freshwater flux in these latitudes can increase the DOHU below 700 m. It can also intensify the strength of thermohaline circulation due to its positive sensitivity to the freshwater flux over the entire Atlantic as indicated in Bugnion (2001).

The OGCM calculations show that the thermohaline circulation in the North Atlantic is reduced by about 5, 1, and 6 Sv (1 Sv = 10^6 m^3 s^{-1}), respectively, when forced with the surface heat flux anomaly only, the freshwater flux anomaly only, and the anomalies of both the surface heat and freshwater fluxes. Indeed, the effect of the anomalous surface heat flux on the thermohaline circulation dominates over that of the anomalous freshwater flux as demonstrated by Kamenkovich et al. (2003). This is also consistent with the result in the ECHAM3 model (Mikolajewicz and Voss 2000) and the second Hadley Centre Coupled Ocean–Atmosphere General Circulation Model (HadCM2; Thorpe et al. 2001), but different from the GFDL model (Dixon et al. 1999).

c. Comparison of buoyancy forcing

Figure 1 shows the changes in the surface heat and moisture fluxes after 70 yr of the global warming scenario with the KSS model. This figure also includes results from seven CMIP-2 models, those from the Bureau of Meteorology Research Centre (BMRC; Power et al. 1993), the Max Planck Institute in Hamburg, Germany (ECHAM3; Cubasch et al. 1997; Voss et al. 1998), the GFDL (Manabe et al. 1991; Manabe and Stouffer 1996), the Goddard Institute for Space Studies (GISS; Russell et al. 1995; Russell and Rind 1999), the Institute of Atmospheric Physics (IAP; Wu et al. 1997; Zhang et al. 2000), the National Center for Atmospheric Research [NCAR; Climate System Model (CSM); Boville and Gent 1998], and the HadCM2 (Johns 1996; Johns et al. 1997). We note that the positions of maximum and minimum $E - P - R$ in the North Atlantic in KSS are slightly different from those in the CMIP-2 models.

However the dominance of the surface heat flux anomaly over the freshwater flux anomaly in the MIT models seems to be consistent with the buoyancy flux anomalies in the CMIP-2 models. As shown in Fig. 2, the buoyancy forcing due to the anomalous surface heat flux decreases about 6 × 10^{-7} kg m^{-2} s^{-1} in the North Atlantic north of 50°N except for the NCAR-CSM model (Fig. 2b). But, the buoyancy forcing due to anomalous freshwater flux decreases merely about 0.5 × 10^{-7} kg m^{-2} s^{-1} in the North Atlantic north of 50°N (Fig. 2d).

As a test of whether the DOHU sensitivities of the MIT adjoint model are reasonably consistent with those of the CMIP-2 models, we use them to estimate DOHU in the CMIP-2 models, and compare the estimates with the DOHU calculated directly from the CMIP-2 data. To make the estimates we average the CMIP-2 surface flux anomalies zonally, but separately for the Pacific and Atlantic basins, and combine them with the adjoint model sensitivities. The results are shown in Table 1. They suggest that, as in our models, DOHU due to anomalous freshwater is very small in the CMIP-2 models.

Table 1 also shows DOHU calculated directly from the CMIP-2 data (ΔT in the table). The model differences are notable (they range from 0.03 to 0.09 K), and represent one reason for the differences between simulations of climate change with different state-of-the-art coupled GCMs (Sokolov and Stone 1998; Raper et al. 2002). Figure 3 illustrates the correlation between DOHU estimated using the MIT adjoint model sensitivities and the actual simulated DOHU. The correlation coefficient, excluding the KSS model, is 0.69, which is significant at the 95% confidence level. Thus the sensitivities of the MIT adjoint model, in spite of its simplifications compared to the CMIP-2 models, appear to be qualitatively similar to those of state-of-the-art coupled GCMs.

4. Sensitivity and mechanisms of deep-ocean heat uptake

a. Sensitivity

As indicated in (5), the sensitivity of DOHU to the net surface heat (Q_S) and freshwater ($F_S = E - P - R$) fluxes obviously depends on the timescale upon which the anomalous forcing acts. In our study of the DOHU below 700 m at the timescale of 70 yr, we run the adjoint model for 70 yr, and calculate the sensitivities for the timescale from 1 to 70 yr. Figure 4 displays the sensitivity of DOHU to the surface heat flux at the timescale of 50 yr. The sensitivity of DOHU to the surface heat flux is positive in both the Pacific and Atlantic except in a small area of the southwestern South Atlantic near the Drake Passage. The positive sensitivity indicates that the heat absorbed at the surface will in part

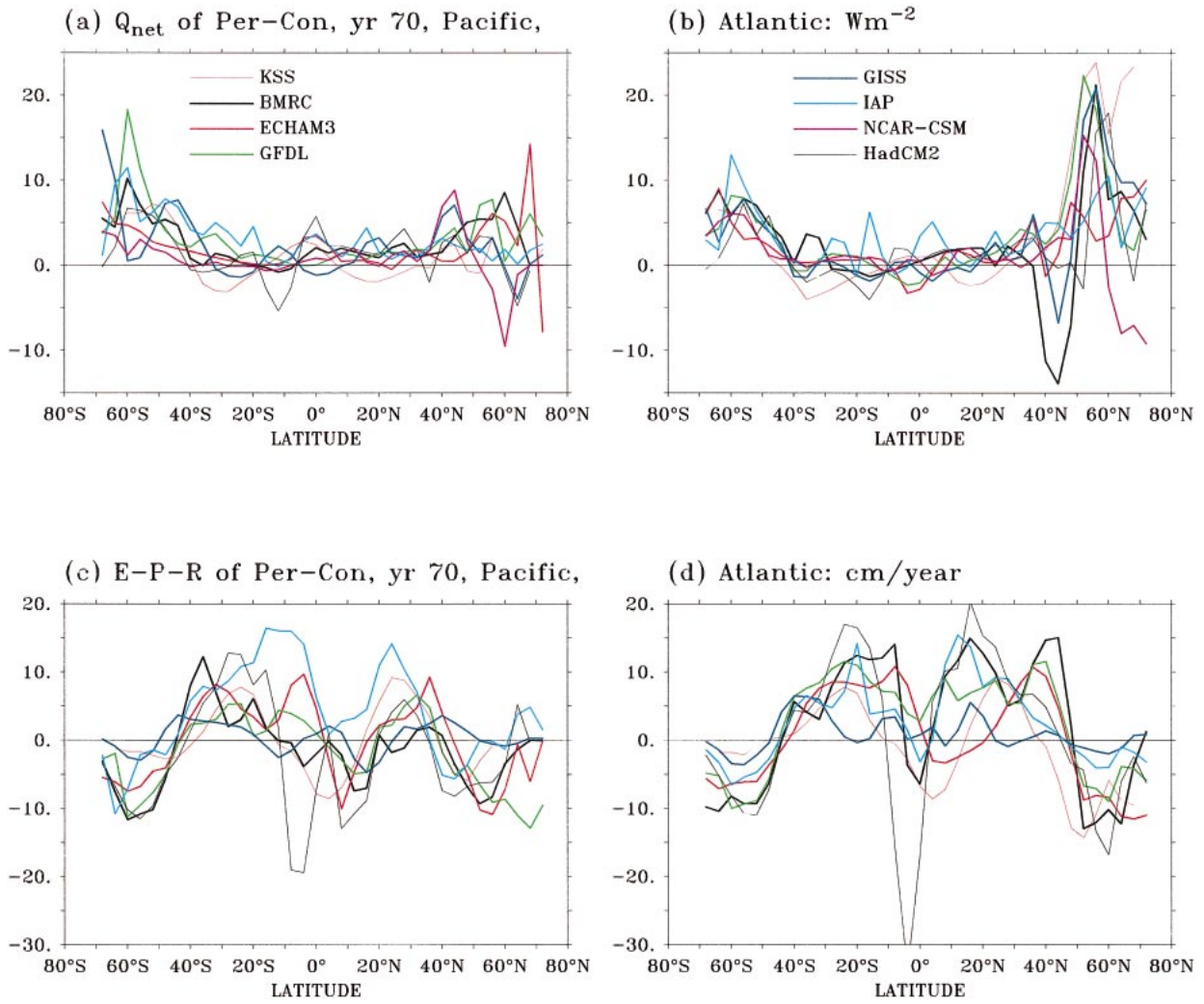

FIG. 1. Zonal averaged mean anomalies between 61 and 80 yr except for KSS, which is the annual average of year 70. Downward net surface heat flux (a) in the Pacific and (b) in the Atlantic in units of W m^{-2}. Freshwater flux ($E - P - R$) (c) in the Pacific and (d) in the Atlantic in units of cm yr^{-1}.

penetrate into the deep ocean and increase the global mean temperature below 700 m. However, the magnitude of the sensitivity is generally larger in the North Atlantic (about 5–20 $\times$ 10^{-6} km^2 W^{-1}) than in the North Pacific (about 5 $\times$ 10^{-6} km^2 W^{-1}), but smaller in the South Atlantic (less than 5 $\times$ 10^{-6} km^2 W^{-1}) than in the South Pacific between 0° and 50°S (about 5–10 $\times$ 10^{-6} km^2 W^{-1}). The sensitivity in the Southern Ocean is the highest (about 20–30 $\times$ 10^{-6} km^2 W^{-1}).

b. Mechanisms

As shown in section 3, the DOHU below 700 m in the global warming scenario of a 1% CO_2 increase per year is mainly determined by the anomaly of surface heat flux. A further question is the following: How does the surface heat flux penetrate into the deep ocean? Obviously, the increase of the DOHU below 700 m must be associated with the increase of the net heat flux (Q_{net}) across 700 m. The net heat flux is the sum of the advective heat flux (Q_W), convective heat flux (Q_{CV}), diapycnal (vertical) diffusive heat flux (Q_{DD}), and diffusive heat flux (isopycnal and thickness diffusion) due to GMR mixing (Q_{GMR}), as in Huang et al. (2003). These heat fluxes are all defined as positive downward, and formulated as follows:

$$Q_W = \rho c_p \iint WT\, dx\, dy, \tag{13}$$

$$Q_{\text{CV}} = \frac{\rho c_p \Delta z_i}{\Delta t}\left(T_i - \frac{T_t \Delta z_i + T_{i+1}\Delta z_{i+1}}{\Delta z_i + \Delta z_{i+1}}\right), \tag{14}$$

$$Q_{\text{DD}} = \rho c_p \iint K_t \frac{\partial T}{\partial z}\, dx\, dy, \tag{15}$$

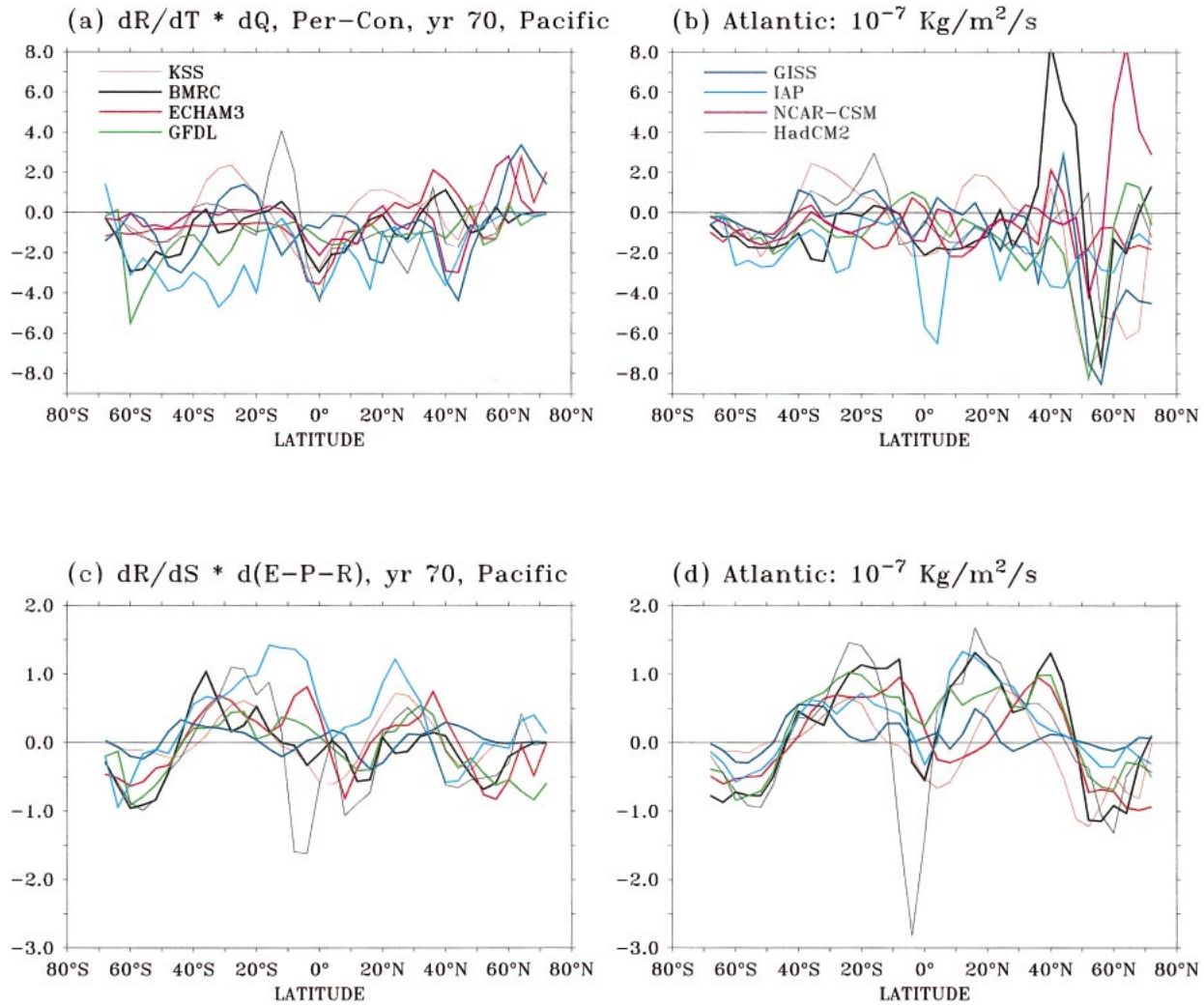

FIG. 2. Buoyancy forcing (positive downward) caused by the anomalous surface heat flux (a) in the Pacific and (b) in the Atlantic, and by the anomalous freshwater flux (c) in the Pacific and (d) in the Atlantic in units of 10^{-7} kg m^{-2} s^{-1}. Values are the zonally averaged mean between 61 and 80 yr except for KSS, which is the annual average for year 70.

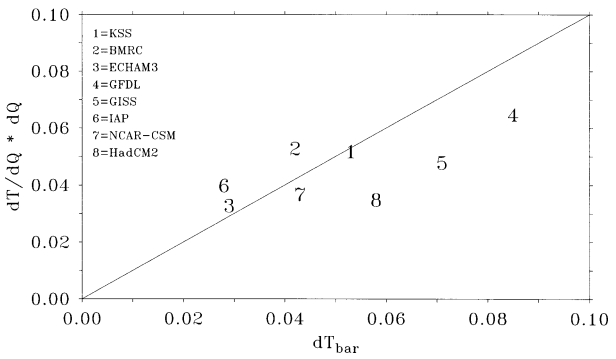

FIG. 3. Comparison of the DOHU below 700 m calculated from CMIP-2 simulations (ΔT, x axis) with that estimated by applying the adjoint sensitivity $(\partial\overline{T}/\partial Q_S)\Delta Q_S$ (y axis).

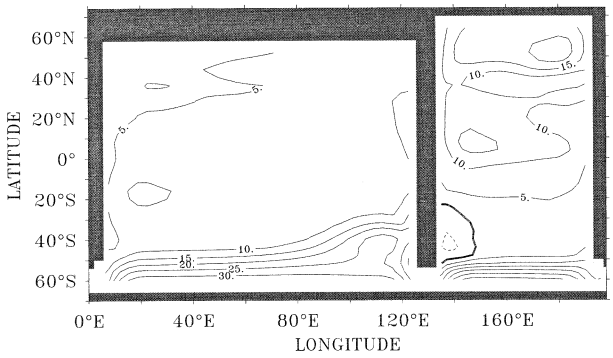

FIG. 4. Sensitivity of DOHU below 700 m to the surface heat flux. Contour interval is 2×10^{-6} km^2 W^{-1}. The solid (dashed) contours represent positive (negative) values. The timescale for the sensitivity is 50 yr.

$$Q_{\mathrm{GMR}} = 2\rho c_p \iint I_t \left[\frac{\partial T}{\partial y}\left(\frac{\partial z}{\partial y}\right)_\sigma + \frac{\partial T}{\partial x}\left(\frac{\partial z}{\partial x}\right)_\sigma \right] dx\, dy, \quad (16)$$

$$Q_{\mathrm{net}} = Q_W + Q_{\mathrm{CV}} + Q_{\mathrm{DD}} + Q_{\mathrm{GMR}}. \quad (17)$$

Here K_t and I_t are diapycnal (vertical) and isopycnal diffusivities of temperature, and $(\partial z/\partial y)_\sigma$ is the slope of the isopycnal surface. The convective heat flux is calculated according to the adjustment of ocean temperature within the adjacent layers when water density is higher in the upper layer than in the lower layer.

To diagnose what physical processes are involved in the DOHU, we take advantage of the adjoint model using these five heat fluxes as so-called cost functions, and calculate the adjoint sensitivities of these five heat fluxes to the surface heat flux (Q_S) as indicated in (5). Figure 5 shows these sensitivities for the timescale of 50 yr. It is clear that the sensitivity of Q_{net} across 700 m to Q_S is positive (Fig. 5a), and is strong in the North Atlantic (about 120×10^9 m^2) and the Southern Ocean (about $60–80 \times 10^9$ m^2). The sign and magnitude of the sensitivity of Q_{net} to Q_S in Fig. 5a are very consistent with those of the sensitivity of DOHU to Q_S in Fig. 4. When the ocean surface is forced with a heat flux anomaly, the downward net heat flux across 700 m will increase, and therefore the deep ocean takes up more heat.

Furthermore, the increase of Q_{net} across 700 m is mainly associated with convective heat flux (Q_{CV}) in the North Atlantic and the heat flux (Q_{GMR}) due to GMR mixing in the Southern Ocean and the North Atlantic. This can be seen by comparing the sign and magnitude of their sensitivities in Figs. 5a,c,e. When the surface heat flux increases, the upper-layer ocean becomes lighter, and therefore convection is prohibited. This means that the upward convective heat flux decreases or that the downward anomaly of convective heat flux increases in the North Atlantic. Since Q_{GMR} is directly associated with the slope of the isopycnal surface as indicated in (16), upward Q_{GMR} mainly occurs in the North Atlantic and the Southern Ocean (not shown) where the slope of the isopycnal surface is very steep. When the surface heat flux increases in these regions, the slope of the isopycnal surface will be flattened. Therefore, the upward eddy heat flux along the isopycnal in the GMR scheme decreases, that is, the downward anomaly of heat flux increases. The effect of isopycnal mixing in the Southern Ocean on the DOHU can also be seen in Gregory (2000). By contrast, in Gregory's study the convection in the North Atlantic did not penetrate as deeply as in ours, and did not affect DOHU at these depths.

The positive sensitivities of net, advective, diapycnal diffusive heat fluxes to the surface heat anomaly in the South Pacific (Figs. 5a,b,d) indicate that the vertical advection (Q_W) and diapycnal diffusion may also contribute to the net heat flux across 700 m. Nevertheless, their effects on the DOHU appear to be small, since the magnitude of anomalous surface heat flux is very small in the South Pacific (Fig. 6b). Overall, the global mean sensitivities of Q_{net}, Q_W, Q_{CV}, Q_{DD}, and Q_{GMR} to the surface heat flux are about 40, 2, 7, 3, and 27 $\times$ 10^9 m^2, respectively, at the timescale of 50 yr, indicating that the DOHU is mainly associated with the reduction of upward GMR mixing.

In addition, we can see that the distribution of Q_W sensitivity to the surface heat flux Q_S (Fig. 5b) is directly associated with the change of the thermohaline circulation (Bugnion 2001; Mikolajewicz and Voss 2000; Dixon et al. 1999). As the surface heat flux increases in the Atlantic, we speculate that the conveyor circulation of downwelling in the Atlantic and upwelling in the Pacific decreases. Therefore, the downward advective heat flux will decrease in the Atlantic, which will lead to a cooling of the deep ocean. In contrast, when the surface heat flux increases in the Pacific, the conveyor circulation will increase. Therefore, the downward advective heat flux will increase, which will result in a warming of the deep ocean.

Since the effect of anomalous freshwater flux on DOHU is negligible in this global warming scenario, we do not discuss the detailed mechanisms by which the freshwater flux affects DOHU. Readers may refer to a similar discussion in Huang et al. (2003) about the mechanisms of DOHU due to freshwater flux for equilibrium states.

5. Characteristics of deep-ocean heat uptake

Calculations in sections 3a,b indicate that after 70 yr in our global warming simulations the total heat absorbed by the ocean is about 60×10^{22} J, and the DOHU below 700 m is about 20×10^{22} J. A further question is, where does the DOHU originate from? We answer this question by using our adjoint sensitivities with the actual surface heat flux changes calculated with the KSS model:

$$E(x, y) = \frac{\rho c_p V_{700}}{\Delta x \Delta y} \sum_{i=1}^{n} \left[\frac{\partial \overline{T}_{n-i+1}}{\partial Q_S(x, y)} \Delta Q_i + \frac{\partial \overline{T}_{n-i+1}}{\partial F_S(x, y)} \Delta F_i \right], \quad n = 1, 70. \quad (18)$$

Here, $E(x, y)$ is the DOHU per unit area, which represents mean heat penetration across 700 m due to the change in the surface heat flux at (x, y). The V_{700} is the ocean volume below 700 m, and ΔQ_i and ΔF_i are from (8) and (9). The effect from the wind stress anomaly is neglected.

As indicated in Fig. 6a, within 70 yr the total heat uptake from the atmosphere in the Pacific north of 40°S (about $2–4 \times 10^9$ J m^{-2}) and the central Atlantic (about $1–2 \times 10^9$ J m^{-2}) is very weak if compared with that over the North Atlantic (about $10–45 \times 10^9$ J m^{-2}) and the Southern Ocean (about $4–8 \times 10^9$ J m^{-2}). We can see (Fig. 6b) that the DOHU across 700 m mainly occurs in the North Atlantic north of 40°N (about $2–15 \times 10^9$ J m^{-2}), the South Atlantic south of 50°S (about $2–6 \times$

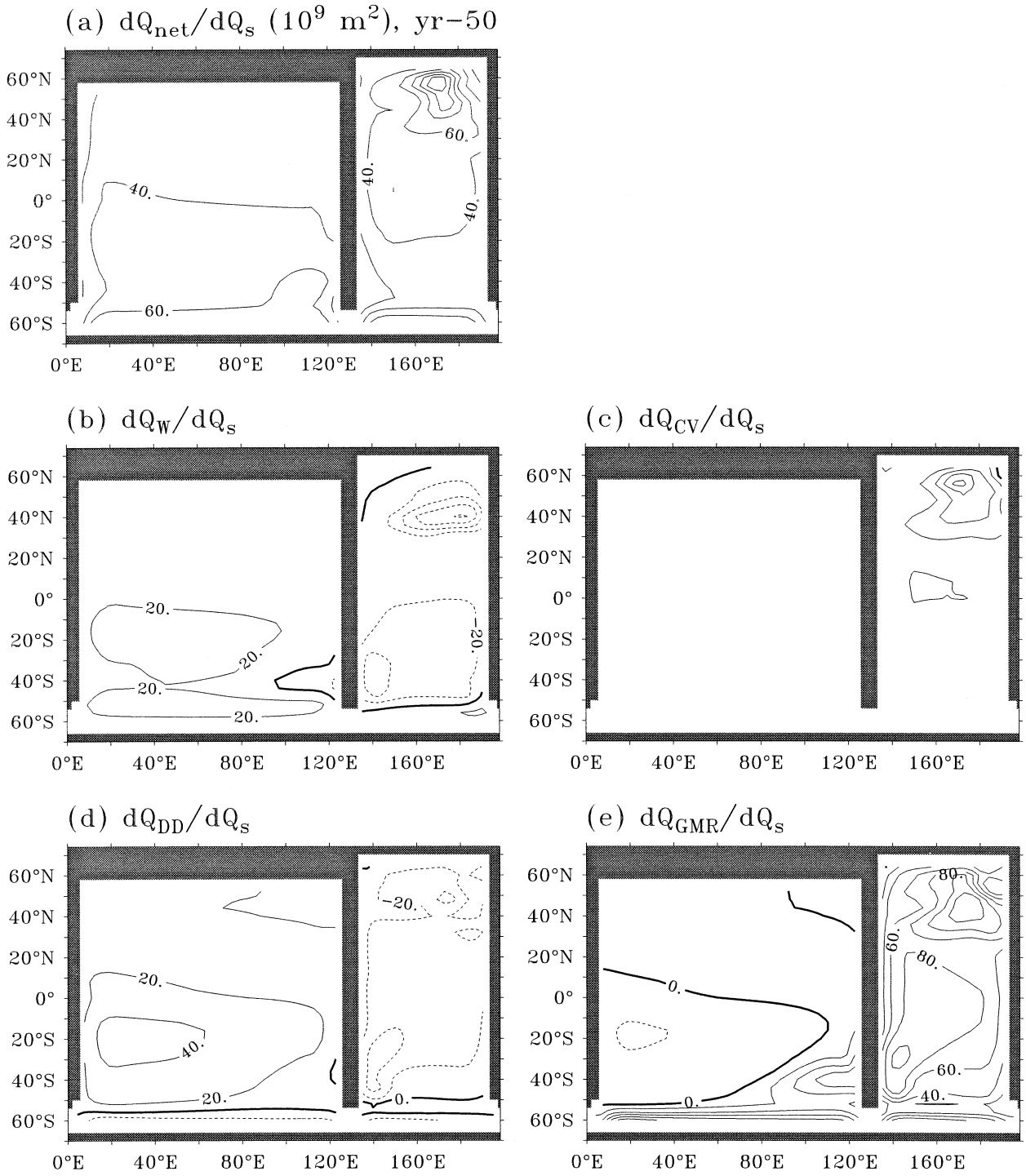

FIG. 5. Adjoint sensitivity of downward heat fluxes across 700 m to the surface heat anomaly at the timescale of 50 yr. (a) Net heat flux, (b) vertical advective heat flux, (c) convective heat flux, (d) diapycnal heat flux, and (e) eddy heat flux due to GMR mixing. The contour interval is 20×10^9 m^{-2}.

10^9 J m^{-2}), and the South Pacific south of 45°S (about 2–4 $\times$ 10^9 J m^{-2}). It appears that the surface heat flux has difficulty penetrating across 700 m into the deep ocean in a large area of the Pacific north of 40°S and the central Atlantic between 50°S and 30°N. Therefore, we can think of a heat sink in the North Atlantic and the Southern Ocean.

We speculate that the heat sink in our OGCM with

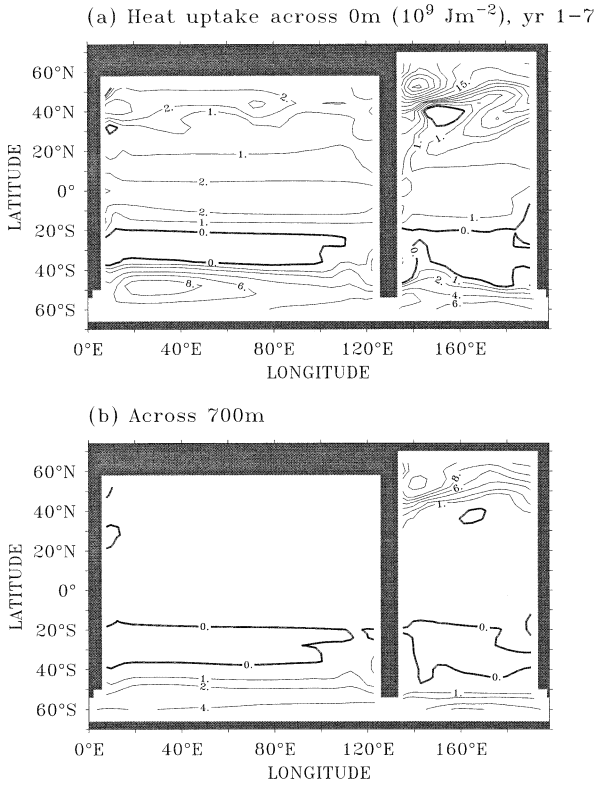

FIG. 6. Ocean heat uptake within 70 yr across (a) 0 and (b) 700 m. Contour intervals are 1 between 0 and 1, 2 between 2 and 10, and 5 between 15 and 50. The unit is 10^9 J m^{-2}.

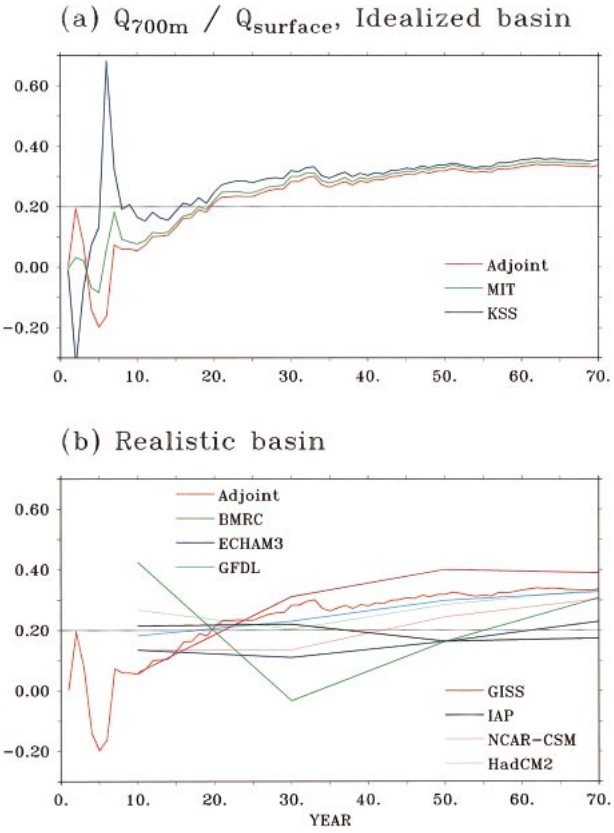

FIG. 7. Ratio between DOHU below 700 m and the total absorbed heat. (a) Models with an idealized basin and (b) models with fully coupled GCMs and a realistic topography from CMIP-2.

an idealized basin may be similar in fully coupled GCMs, although its strength and width distribution will not be identical. For example, as indicated in Figs. 1a,b, the heat flux anomaly at the ocean surface is mainly located in the North Atlantic north of 50°N and the Southern Ocean south of 40°S in almost all fully coupled GCMs with realistic topography, as well as in the coupled model with an idealized basin from KSS. However, a weak heat sink may also exist in the North Pacific north of 50°N such as in the study of Gregory (2000) using the HadCM2 model as indicated in Fig. 1a.

Next we compare the heat uptake below 700 m with total absorbed heat,

$$R_n = \frac{\text{DOHU}}{Q_0}, \qquad n = 1, 70, \tag{19}$$

where

$$Q_0 = \int \sum_{i=1}^{n} Q_i \Delta t_i \, dx \, dy, \tag{20}$$

is the total heat absorbed by the ocean within n years, Q_i is the heat flux anomaly at year i, and Δt_i is the time interval between the model outputs of Q_i and Q_{i+1}. In the adjoint model, DOHU is estimated as

$$\text{DOHU} = \int E(x, y) \, dx \, dy, \tag{21}$$

which is the global integration of (18). Calculation indicates that the ratio R_n is about 10%–20% during years 10–20, and gradually increases to about 33% as indicated in Fig. 7a, which is consistent with the result of Gregory (2000). The large fluctuation of the ratio in the first 10 yr is purely due to the fact that Q_0 is almost near zero, and the ratio is very noisy.

The ratio estimated from the adjoint model is confirmed by the simulation of the MIT OGCM and the original simulation of KSS, where the DOHU is calculated using

$$\text{DOHU} = \rho c_p V_{700} \Delta \overline{T}_n. \tag{22}$$

Here, $\Delta \overline{T}_n$ is the mean temperature difference below 700 m between the perturbation and control run as shown in (12). It is clear that the ratio R_n is very close in all three models. The ratios R_n in the original simulation of the fully coupled GCMs from CMIP-2 with a realistic topography are also calculated using Eqs. (12), (19), and (22), since the heat uptake due to the change of sea ice heat content is trivial and neglected. These ratios are about 10%–30% during the first 20 yr, and gradually increase to about 20%–40% during the fourth 20-yr period (Fig. 7b). The fluctuation of these ratios might be

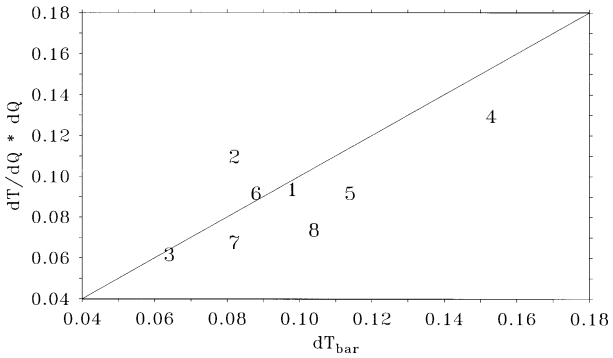

FIG. 8. Comparison of the DOHU below 200 m calculated by applying OGCM simulation ΔT (x axis) with that estimated by applying adjoint sensitivity $(\partial\overline{T}/\partial Q_S)\Delta Q_S$ (y axis). The figure legends are the same as in Fig. 3.

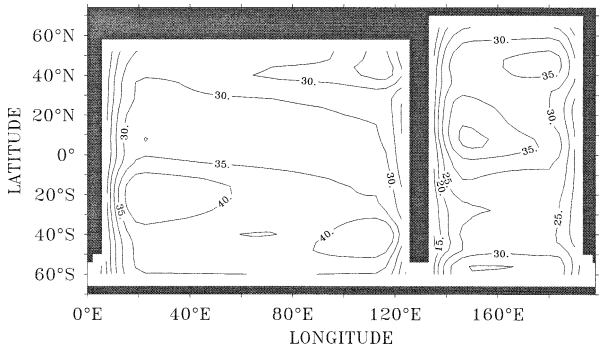

FIG. 9. Sensitivity of DOHU below 200 m to the surface heat flux. Contour interval is 5×10^{-6} km^2 W^{-1}.

associated with different vertical diffusivities applied in these models.

6. Heat uptake below 200 m

The characteristics of the DOHU below 200 m in the global warming scenario with a 1% CO_2 increase per year for 70 yr are very similar to those of the DOHU below 700 m. The DOHU below 200 m (about 0.1 K) based on the adjoint sensitivities and OGCM simulation with an idealized basin are very close (Table 1), indicating the linearity of the response of DOHU to the surface heat flux. The DOHU estimated in the idealized basin is in the middle of that calculated in the realistic basin of the CMIP-2 models (about 0.06–0.15 K). The DOHU estimated by applying the adjoint sensitivity is well correlated with that calculated in the coupled models of CMIP-2 (Fig. 8). The correlation excluding the KSS model is 0.73, which corresponds to a better than 95% confidence level. The effect of anomalous surface freshwater flux on the DOHU below 200 m appears to be negligible (Table 1).

The adjoint sensitivity of DOHU below 200 m to the surface heat flux is positive over both the Pacific and the Atlantic (Fig. 9) as for that below 700 m in Fig. 4. The main difference is that the magnitude of sensitivity of the DOHU below 200 m is higher and more uniformly distributed than that below 700 m.

The heat flux across 200 m is associated in part with the reduction of convection in the North Atlantic, which is consistent with Gregory (2000). However, Gregory (2000) shows that the increase of vertical diffusion contributes a lot to the heat flux near 200 m in both the North Pacific and North Atlantic, which differs from our result. Rather, our study indicates that the reduction of the GMR mixing is the main contributor to the vertical heat flux in the North Atlantic. This may be associated with the different subgrid-scale eddy parameterizations; that is, Gregory (2000) used diapycnal diffusion with its coefficient increasing with depth, and we use GMR mixing in addition to diapycnal diffusion with a constant coefficient.

The DOHU below 200 m can be traced back to the regions of the heat sink in the North Atlantic and in the Southern Ocean as for the DOHU below 700 m. However, the magnitude of DOHU increases to 30×10^9 J m^{-2} in the North Atlantic north of 40°N and to $4–6 \times 10^9$ J m^{-2} in the Southern Ocean south of 40°S (Fig. 10).

The ratio of heat uptake below 200 m to the total heat uptake is shown in Fig. 11. The ratios of DOHU estimated in the adjoint model, MIT OGCM, and KSS model are very close; they are about 20%–50% at the timescale of 10 yr and gradually increase to about 70% at the timescale of 70 yr. (Fig. 11a). These ratios are also consistent with those from the fully coupled GCMs of CMIP-2 (Fig. 11b), which range from 10% to 60% at a 10-yr timescale and from 60% to 70% at a 70-yr timescale. The surface heat flux into the ocean in this global warming scenario is almost equally (about one-third) absorbed by the upper ocean above 200 m, between 200 and 700 m, and below 700 m. These ratios are close to those in the study of Gregory (2000).

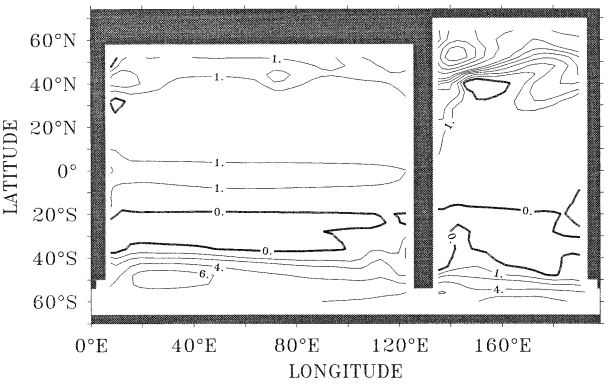

FIG. 10. Ocean heat uptake across 200 m at a timescale of 70 yr. Contour intervals are 1 between 0 and 1, 2 between 2 and 10, and 5 between 15 and 50. The unit is 10^9 J m^{-2}.

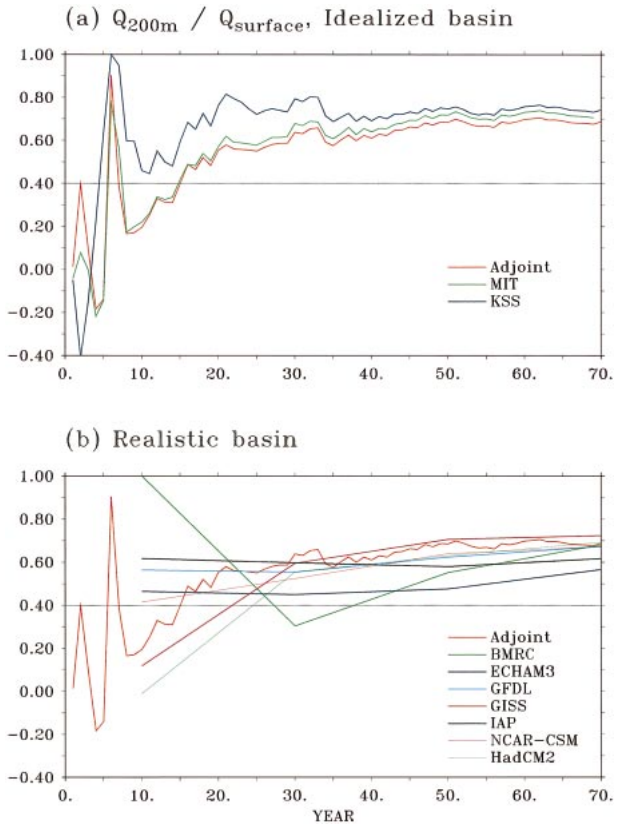

FIG. 11. Ratio between DOHU below 200 m and the total absorbed heat. (a) Models with an idealized basin and (b) models with fully coupled GCMs and a realistic topography from CMIP-2.

7. Conclusions

We have studied the DOHU using simulations with the MIT OGCM and its adjoint with an idealized geometry. The simulations are forced with the anomalous surface heat and freshwater fluxes from the coupled model of KSS in a global warming scenario where atmospheric CO_2 increases 1% yr^{-1} for 70 yr. The DOHU in our simulations are compared with that in the fully coupled AOGCMs of CMIP-2.

We find that the contribution of anomalous freshwater fluxes to DOHU in our models is negligible. This is in part due to the relatively small contribution of the freshwater flux anomalies to the buoyancy flux anomalies in the KSS global warming scenario. We found that the buoyancy flux anomalies in all the CMIP-2 coupled GCMs were also dominated by the heat flux anomalies, and that the DOHU in the CMIP-2 models were well correlated with DOHU estimates based on the MIT adjoint model sensitivities. Thus the DOHU in the CMIP-2 models appears to have qualitatively similar sensitivities.

The sensitivity of DOHU to the downward surface heat flux in the adjoint model is positive in both the Pacific and Atlantic, but it is strongest in the North Atlantic and the Southern Ocean. The increase of DOHU is largely associated with the reduction of convective activity due to surface heating and the reduction of GMR mixing due to flattening of the isopycnal slopes in the North Atlantic. The reduction of GMR mixing is the main contributor to the increase of the DOHU in the Southern Ocean. The dominance of the heat sinks arises because the sensitivity of DOHU to heat flux perturbations and the anomalies in the surface heat fluxes in the global warming scenario are both particularly large in these regions. We would expect qualitatively similar heat sinks to occur in coupled GCMs with similar physics.

The heat absorption of the ocean in our models is almost equally (one-third) distributed above 200 m, between 200 and 700 m, and below 700 m. After 70 yr of the global warming scenario, the DOHU below 700 m is about 20×10^{22} J, or 0.05 K. In the coupled GCMs of CMIP-2, this latter number varies from 0.03 to 0.09 K. In the MIT OGCM the heat uptake in the 70 yr of the global warming scenario is to a very good approximation a linear response to the surface heat flux changes.

Acknowledgments. The authors thank Dr. Jonathan M. Gregory and other two anonymous reviewers for their critiques and comments, which helped to improve our manuscript.

REFERENCES

Barnett, T. P., D. W. Pierce, and R. Schnur, 2001: Detection of anthropogenic climate change in the world's oceans. *Science,* **292,** 270–274.

Boville, B. A., and P. R. Gent, 1998: The NCAR Climate System Model, Version One. *J. Climate,* **11,** 1115–1130.

Bugnion, V., 2001: Driving the ocean's overturning: Analysis with adjoint models. Ph.D. dissertation, Massachusetts Institute of Technology, 179 pp. [Available from Lindgren Library, MIT Building 54, 77 Massachusetts Ave., Cambridge, MA 02139.]

Cubasch, U., R. Voss, G. C. Hegerl, J. Waszkewitz, and T. J. Crowley, 1997: Simulation of the influence of solar radiation variations on the global climate with an ocean–atmosphere general circulation model. *Climate Dyn.,* **13,** 757–767.

Dixon, K. W., T. L. Delworth, M. J. Spelman, and R. J. Stouffer, 1999: The influence of transient surface fluxes on North Atlantic overturning in a coupled GCM climate change experiment. *Geophys. Res. Lett.,* **26,** 2749–2752.

Gent, P. R., and J. C. McWilliams, 1990: Isopycnal mixing in ocean circulation models. *J. Phys. Oceanogr.,* **20,** 150–155.

Giering, R., 1999: Tangent linear and adjoint model compiler, users manual. Max-Planck Institut, Hamburg, Germany, 64 pp.

Gregory, J. M., 2000: Vertical heat transports in the ocean and their effect on time-dependent climate change. *Climate Dyn.,* **16,** 501–515.

Huang, B., P. H. Stone, and C. Hill, 2003: Sensitivities of deep-ocean heat uptake and heat content to the surface fluxes and subgrid-scale parameters in an OGCM with idealized geometry. *J. Geophys. Res.,* **108,** 3015, doi: 10.1029/2001JC001218.

Jiang, S., P. H. Stone, and P. Malanotte-Rizzoli, 1999: An assessment of the Geophysical Fluid Dynamics Laboratory ocean model with coarse resolution: Annual-mean climatology. *J. Geophys. Res.,* **104,** 25 623–25 645.

Johns, T. C., 1996: A description of the Second Hadley Centre Coupled Model (HadCM2). Climate Research Tech. Note 71, 19 pp.

[Available from Hadley Centre, Met Office, Bracknell, Berkshire RG12 2SY, United Kingdom.]

——, R. E. Carnell, J. F. Crossley, J. M. Gregory, J. F. B. Mitchell, C. A. Senior, S. F. B. Tett, and R. A. Wood, 1997: The second Hadley Centre coupled ocean–atmosphere GCM: Model description, spinup and validation. *Climate Dyn.,* **13,** 103–134.

Kamenkovich, I. V., A. Sokolov, and P. H. Stone, 2002: A coupled atmospheric–ocean model of intermediate complexity for climate change. *Climate Dyn.,* **19,** 585–598.

——, ——, and ——, 2003: Feedbacks affecting the response of the thermohaline circulation to increasing CO_2: A study with a model of intermediate complexity. *Climate Dyn.,* in press.

Latif, M., E. Roeckner, U. Mikolajewicz, and R. Voss, 2000: Tropical stabilization of the thermohaline circulation in a greenhouse warming simulation. *J. Climate,* **13,** 1809–1813.

Levitus, S., J. I. Antonov, T. P. Boyer, and C. Stephens, 2000: Warming of the world ocean. *Science,* **287,** 2225–2229.

——, ——, J. Wang, T. L. Delworth, K. W. Dixon, and A. J. Broccoli, 2001: Anthropogenic warming of Earth's climate system. *Science,* **292,** 267–270.

Manabe, S., and R. J. Stouffer, 1996: Low-frequency variability of surface air temperature in a 1000-year integration of a coupled ocean–atmosphere model. *J. Climate,* **9,** 376–393.

——, ——, M. J. Spelman, and K. Bryan, 1991: Transient responses of a coupled ocean–atmosphere model to gradual changes of atmospheric CO_2. Part I: Annual mean response. *J. Climate,* **4,** 785–818.

Marotzke, J., R. Giering, K. Q. Zhang, D. Stammer, C. Hill, and T. Lee, 1999: Construction of the adjoint MIT ocean general model and application to Atlantic heat transport sensitivity. *J. Geophys. Res.,* **104,** 29 529–29 547.

Marshall, J., A. Adcroft, C. Hill, L. Perelman, and C. Heisey, 1997: A finite volume, incompressible Navier Stokes model for studies of the ocean on parallel computers. *J. Geophys. Res.,* **102,** 5753–5766.

Mikolajewicz, U., and R. Voss, 2000: The role of the individual air–sea flux components in CO_2-induced changes of the ocean's circulation and climate. *Climate Dyn.,* **16,** 627–642.

Power, S. B., R. A. Colman, B. J. McAvaney, R. R. Dahni, A. M. Moore, and N. R. Smith, 1993: The BMRC coupled atmosphere/ocean/sea-ice model. BMRC Research Rep. 37, Bureau of Meteorology Research Centre, Melbourne, Australia, 58 pp.

Rahmstorf, S., 1995: Bifurcation of the Atlantic thermohaline circulation in response to changes in the hydrological cycle. *Nature,* **378,** 145–149.

——, 1996: On the freshwater forcing and transport of the Atlantic thermohaline circulation. *Climate Dyn.,* **12,** 799–811.

——, and A. Ganopolski, 1999: Long-term global warming scenarios computed with an efficient coupled climate model. *Climatic Change,* **43,** 353–367.

Raper, S. C. B., J. M. Gregory, and R. J. Stouffer, 2002: The role of climate sensitivity and ocean heat uptake on AOGCM transient temperature response. *J. Climate,* **15,** 124–130.

Redi, M. H., 1982: Oceanic isopycnal mixing by coordinate rotation. *J. Phys. Oceanogr.,* **12,** 1154–1158.

Russell, G. L., and D. Rind, 1999: Response to CO_2 transient increase in the GISS coupled model: Regional coolings in a warming climate. *J. Climate,* **12,** 531–539.

——, J. R. Miller, and D. Rind, 1995: A coupled atmosphere–ocean model for transient climate change studies. *Atmos.–Ocean,* **33,** 683–730.

Sokolov, A., and P. H. Stone, 1998: A flexible climate model for use in integrated assessments. *Climate Dyn.,* **14,** 291–303.

Thorpe, R. B., J. M. Gregory, T. C. Johns, R. A. Wood, and J. F. B. Mitchell, 2001: Mechanisms determining the Atlantic thermohaline circulation response to greenhouse gas forcing in a non-flux-adjusted coupled climate model. *J. Climate,* **14,** 3102–3116.

Voss, R., R. Sausen, and U. Cubasch, 1998: Periodically synchronously coupled integrations with the atmosphere–ocean general circulation model ECHAM3/LSG. *Climate Dyn.,* **14,** 249–266.

Weaver, A., J. Marotzke, P. E. Cummins, and E. S. Sarachik, 1993: Stability and variability of the thermohaline circulation. *J. Phys. Oceanogr.,* **23,** 39–60.

Wiebe, E. C., and A. J. Weaver, 1999: On the sensitivity of global warming experiments to the parameterisation of sub-grid scale ocean mixing. *Climate Dyn.,* **15,** 875–893.

Wu, G.-X., and Coauthors,1997: Global ocean–atmosphere–land system model of LASG (GOALS/LASG) and its performance in simulation study (in Chinese). *Quart. J. Appl. Meteor.,* **8** (Suppl.), 15–28.

Zhang, J., R. W. Schmitt, and R. X. Huang, 1999: The relative influence of diapycnal mixing and hydrological forcing on the stability of the thermocline circulation. *J. Phys. Oceanogr.,* **29,** 1096–1108.

Zhang, X.-H., G.-Y. Shi, H. Liu, and Y.-Q. Yu, Eds., 2000: *IAP Global Atmosphere–Land System Model.* Science Press, 259 pp.